

Electronic origin of ferroic quadrupole moment under antiferroic quadrupole orders and finite magnetic moment in $J_{\text{eff}} = 3/2$ systems

Haruhiro Kubo, Takayuki Ishitobi, and Kazumasa Hattori

*Department of Physics, Tokyo Metropolitan University,
1-1, Minami-osawa, Hachioji, Tokyo 192-0397, Japan*

(Dated: July 6, 2023)

We study the electronic origin of parasitic ferroic quadrupole moments in antiferroic quadrupole orders by extending a model studied in G. Chen et al., Phys. Rev. B **82**, 174440 (2010) with the effective angular momentum $J_{\text{eff}} = 3/2$ quartet ground states. Taking into account the first crystalline-electric-field (CEF) excited doublet, cubic anisotropy in the quadrupole moments emerges, which leads to the induced ferroic quadrupole moments in the antiferro quadrupolar phases. The hybridization with the CEF excited quartet states also causes finite magnetic moments compatible to the observed size of the effective moment in typical $J_{\text{eff}} = 3/2$ systems, as opposed to the naive expectation of vanishing moments in the $J_{\text{eff}} = 3/2$ systems. These results suggest the importance of the corrections arising from the high-energy CEF excited states in the $J_{\text{eff}} = 3/2$ systems.

I. INTRODUCTION

Strongly correlated electrons systems with orbital degrees of freedom have attracted great attention in recent years¹. The orbital degrees of freedom possess potential functions alternative to the modern magnetic-based devices². Combining the orbital and conventional spin degrees of freedom inevitably leads to the notion of multipole moments³. Such multipole moments play important role in correlated electron systems with strong spin-orbit couplings. They can exhibit various fascinating phenomena such as topological spin-orbital Mott insulators⁴, spin-orbital liquid states^{5–8}, superconductivity mediated by multipolar spin-orbital fluctuations^{9,10}, and in doped Mott insulators¹¹.

For activating multipole physics, one needs high symmetry and strong spin-orbit couplings. Possible candidates are Mott insulators with d^1 configuration surrounded by a regular oxygen octahedron. Although materials with $3d$ electrons often exhibit the Jahn-Teller distortion as lowering temperature, some $5d$ electron systems keep their cubic symmetry even at low temperatures. As a such d electron system, double-perovskite compounds A_2BTrO_6 ($A=\text{Ba, Sr, Ca}$; $B=\text{Mg, Ca, Sr, Ba, Zn, Cd}$, $Tr=\text{Re, Os, Mo}$)^{12–22} and Ta chlorides $A_2\text{TaCl}_6$ ($A=\text{K, Rb, Cs}$)²³ have been recently studied intensively. The oxygen octahedron crystalline-electric-field (CEF) lifts the ten-fold degeneracy of the d electrons to the high-energy e_g and the low-energy t_{2g} states. The latter is split further by the spin-orbit coupling and form so-called effective angular momentum $J_{\text{eff}} = 3/2$ ground state and $J_{\text{eff}} = 1/2$ first excited state. In these compounds, the spin-orbit coupling λ is of the order of $\sim 0.2\text{--}0.4$ eV, while the CEF gap between the ground t_{2g} and the excited e_g states D is $D \sim 3\text{--}5$ eV^{23–25}.

What is unique to these systems is that the ground state with $J_{\text{eff}} = 3/2$ has no magnetic dipole moment as a result of exact cancellation between the spin and orbital angular momenta. This leads to various possibilities of multipole orders at low temperatures. For ex-

ample, Re based double-perovskites exhibit ferro and antiferro quadrupole orders in addition to dipole-octupole magnetic orders. In $\text{Ba}_2\text{TrOsO}_6$ ($Tr=\text{Zn, Mg, and Ca}$) with d^2 configuration, octupole orders have been suggested recently.^{26,27}

The vanishing magnetic dipole moment is also reflected in the small moment typically $\sim 0.3\text{--}0.8\mu_B$ in their high-temperature magnetic susceptibility, where μ_B is the Bohr magneton. This small but finite value has been interpreted as a partial cancellation of the spin and orbital angular momenta owing to the hybridization between the d and the oxygen p orbitals.^{22,23,28}

In the pioneering work by Chen et al.,²⁹ a model containing the ground-state CEF quartet originating from the t_{2g} orbital was constructed in the limit of the strong spin-orbit coupling $\lambda \rightarrow \infty$. The quartet can be described by the effective angular momentum $J_{\text{eff}} = 3/2$ and they predicted several interesting multipolar ordered states in terms of the multipole moments of the $J_{\text{eff}} = 3/2$ multiplet: an antiferroic quadrupole order with the e_g irreducible representation and ferro- and antiferro-magnetic dipole-octupole orders. These results are indeed supported by the experimental observation of the phase transitions e.g., in $\text{Ba}_2\text{MgReO}_6$ ²² and $\text{Ba}_2\text{NaOsO}_6$.³⁰

Recently, Hirai et al., reported that ferroic quadrupole moments $\sim O_{20} = 3z^2 - r^2$ emerge under the antiferroic order of the type $O_{22} = x^2 - y^2$ below $T_q = 33$ K by their x-ray experiments³¹. The presence of the ferroic moment can be understood by a simple symmetry argument; the free energy for the e_g orbital moments contains a cubic coupling $\sim O_{22}^2 O_{20}$. This induces ferroic quadrupole moments proportional to the square of the antiferroic ones. They discuss this can be due to the Jahn-Teller effects and the lattice anharmonicity. The former has been recently analyzed and successfully reproduced the emergence of the ferroic quadrupole moments³².

In this paper, we point out that d electron CEF excited states can influence the CEF ground quartet with $J_{\text{eff}} = 3/2$, which has no magnetic dipole moment and no cubic coupling $\sim O_{22}^2 O_{20}$ without couplings to other degrees of freedom. In the $J_{\text{eff}} = 3/2$ multiplets, the lo-

cal cubic anisotropy which arises from the CEF potential vanishes. The anisotropy can emerge when the CEF excited states are taken into account. Such anisotropy due to the excited spin-singlet state (Γ_1 in the cubic symmetry) are indeed discussed in the Γ_3 non-Kramers doublet ground state in Pr-based compounds³³⁻³⁷ and the analysis there is also applicable to the case of the d^1 systems. This is because the $J_{\text{eff}} = 3/2$ states is classified as Γ_8 irreducible representation (irrep) in the cubic symmetry and can be regarded as a product of the spin-1/2 and the orbital $e_g(\Gamma_3)$. Indeed, the CEF first-excited state is the Γ_7 state which is the spin-1/2 and the orbital-singlet state. Thus, apart from the spin degrees of freedom, the orbital sector is identical in the two systems. For the small but finite magnetic dipole moment, it will be shown that the corrections of order $\lambda/D \sim 0.1$ leads to non-negligible contribution to the magnetic moment in realistic systems in this paper.

This paper is organized as follows. In Sec. II, we review the model proposed in Ref. 29 and explicitly introduce the matrix form of quadrupole operators including the excited states. The exchange Hamiltonian is rewritten in terms of these quadrupole and spin-orbital operators to make this paper self-contained form. In Sec. III, we show the results of the two-site mean-field approximation. We discuss the effects of the excited CEF state on the ferro components of the order parameter in the antiferro quadrupole ordered state and also on the phase-diagram. The temperature-magnetic field phase diagrams are also analyzed. In Sec. IV, we discuss the results in this paper and related materials. We also discuss how the finite magnetic moment emerges in the ground state $J_{\text{eff}} = 3/2$ state. Finally, Sec. V summarizes this paper.

II. MODEL

We start by introducing the general model describing d^1 electron configuration for arbitrary spin-orbit coupling and CEF strength. This means that both t_{2g} and e_g degrees of freedom together with the spin 1/2 ones are taken into account. We then derive an effective t_{2g} -dominant model with six states, ignoring the excited e_g dominant states. The interaction between the effective t_{2g} electrons are introduced as similarly to the study in Ref. 29. We will not project them onto the effective total angular momentum $J_{\text{eff}} = 3/2$, but keep both $J_{\text{eff}} = 3/2$ and 1/2 constructed by the t_{2g} orbitals.

A. Local Hamiltonian

The local part of the Hamiltonian is a conventional one with the CEF parameter B_4 and the spin-orbit coupling $\lambda > 0$ as

$$H_{\text{loc}} = H_{\text{CEF}} + H_{\text{SO}}, \quad (1)$$

$$H_{\text{CEF}} = \frac{B_4}{2} \sum_{i,\sigma,m,m'} \gamma_{mm'} d_{m\sigma}^\dagger d_{m'\sigma}, \quad (2)$$

$$H_{\text{SO}} = \lambda \sum_{i,\sigma,m,m'} (\mathbf{L})_{mm'} \cdot \mathbf{s}_{\sigma\sigma'} d_{m\sigma}^\dagger d_{m'\sigma'}, \quad (3)$$

Here, $d_{m\sigma}$ is the d electron annihilation operator with the z component of the orbital angular momentum $m = 0, \pm 1, \pm 2$ and the spin $\sigma = \uparrow, \downarrow$. The CEF potential for the d electrons are parameterized by $\gamma_{mm'} \equiv (\frac{15}{2}m^2 - \frac{35}{2}|m| + 6)\delta_{m,m'} + 5\delta_{|m-m'|,4}$, where $\delta_{m,m'}$ is the Kronecker delta. \mathbf{L} and \mathbf{s} are the orbital angular momentum and the spin-1/2 matrices for the d electrons, respectively.

The eigenstates of H_{loc} are split into $4+2+4$ and their eigenvalues are given as

$$\epsilon_{1/2} = -2B_4 + \lambda, \quad (4)$$

$$\epsilon_{3/2} = \frac{1}{4} \left(2B_4 - \lambda - \sqrt{5} \sqrt{20B_4^2 + 4B_4\lambda + 5\lambda^2} \right), \quad (5)$$

$$\epsilon'_{3/2} = \frac{1}{4} \left(2B_4 - \lambda + \sqrt{5} \sqrt{20B_4^2 + 4B_4\lambda + 5\lambda^2} \right), \quad (6)$$

where the subscripts represent the effective angular momenta; $3/2$ ($1/2$) corresponds to Γ_8 (Γ_7) state in the cubic point group O_h .

For small λ/B_4 with $B_4 > 0$,

$$\epsilon_{3/2} \simeq -2B_4 - \frac{\lambda}{2} - \frac{3\lambda^2}{10B_4} + \dots, \quad (7)$$

$$\epsilon'_{3/2} \simeq 3B_4 + \frac{3\lambda^2}{10B_4} + \dots. \quad (8)$$

When the CEF potential is sufficiently large, $\epsilon'_{3/2}$ is much larger than the other two and the excitation gap D is $D \simeq 5B_4 \sim 3-5$ eV for the compounds mentioned in the Introduction.²³⁻²⁵ Thus, the quartet with its eigenenergy $\epsilon_{3/2}$ corresponds to the ground state with $J_{\text{eff}} = 3/2$ and the first excited state is that with $\epsilon_{1/2}$. The former approximately consists of the t_{2g} electrons, while the latter is purely t_{2g} origin, see Appendix A. In the following, we will concentrate on these six states and ignore the higher energy states at $\epsilon'_{3/2}$. The matrices which will be shown in the following [Eqs. (9),(11), and (12)] are calculated within the full ten-dimensional Hilbert space with keeping $O(\varepsilon^2)$ terms for later purposes. The six states can be labeled by the diagonal elements of the total angular momentum J_z for small $\varepsilon \equiv \lambda/B_4 \sim 0.5$:

$$J_z \simeq \frac{1}{3} \begin{bmatrix} \frac{5}{2} & 0 & -2\sqrt{2} + \alpha_J & 0 & 0 & 0 \\ & -\frac{5}{2} & 0 & -2\sqrt{2} + \alpha_J & 0 & 0 \\ & & \frac{1}{2} + \beta_J & 0 & 0 & 0 \\ & & 0 & -\frac{1}{2} - \beta_J & 0 & 0 \\ & & & & & -\frac{3}{2} \\ & & & & & \frac{3}{2} \end{bmatrix}. \quad (9)$$

Here the empty parts in the matrix have been omitted since $J_z = J_z^\dagger$. The constants α_J and β_J are

given as $\alpha_J = \frac{3\sqrt{2}}{5}\varepsilon + O(\varepsilon^3)$, $\beta_J = \frac{12}{5}\varepsilon - \frac{9}{25}\varepsilon^2 + O(\varepsilon^3)$. Note that the factor 1/3 in Eq. (9) and the basis of the matrix J_z is the eigenstates for $H_{\text{loc}} = \text{diag}(\epsilon_{1/2}, \epsilon_{1/2}, \epsilon_{3/2}, \epsilon_{3/2}, \epsilon_{3/2}, \epsilon_{3/2})$. See the wavefunctions in Appendix A. From this expression, it is clear that the quartet can be described by the effective angular momentum $J_{\text{eff}} = 3/2$ with $J_{\text{eff}}^z = 3J_z$ when the excited states are ignored for $\lambda \rightarrow \infty$ with $\varepsilon = \lambda/B_4 \rightarrow 0$.

For later purposes, it is useful to show the operators constructed by the t_{2g} occupation number n_{xy} , n_{yz} , and n_{zx} ; $n \equiv n_{xy} + n_{yz} + n_{zx}$, $u \equiv 2n_{xy} - n_{yz} - n_{zx}$, and $v \equiv \sqrt{3}(n_{yz} - n_{zx})$.

$$n \simeq \text{diag}(1, 1, 1 - \delta, 1 - \delta, 1 - \delta, 1 - \delta), \quad (10)$$

$$u \simeq \begin{bmatrix} 0 & 0 & \frac{2-\delta}{\sqrt{2}} & 0 & 0 & 0 \\ 0 & 0 & -\frac{2-\delta}{\sqrt{2}} & 0 & 0 & 0 \\ & 1-\delta & 0 & 0 & 0 & 0 \\ & & 1-\delta & 0 & 0 & 0 \\ & & & -1+\delta & 0 & 0 \\ & & & & -1+\delta & 0 \end{bmatrix}, \quad (11)$$

$$v \simeq \begin{bmatrix} 0 & 0 & 0 & 0 & \frac{2-\delta}{\sqrt{2}} & 0 \\ 0 & 0 & 0 & 0 & 0 & \frac{2-\delta}{\sqrt{2}} \\ & 0 & 0 & -1+\delta & 0 & 0 \\ & & 0 & 0 & 1-\delta & 0 \\ & & & 0 & 0 & 0 \\ & & & & 0 & 0 \end{bmatrix}, \quad (12)$$

where $\delta = \frac{3}{50}\varepsilon^2 + O(\varepsilon^3)$, and as similarly to Eq. (9), we have omitted the lower triangle part. For $\delta \rightarrow 0$, $n \rightarrow \mathbb{1}$ (an identity matrix) and e_g quadrupole moments (u, v) are reduced to the quadrupole moments (q_u, q_v) constructed by the angular momentum \mathbf{L} as

$$q_u = \frac{2L_z^2 - L_x^2 - L_y^2}{3}, \quad q_v = \frac{\sqrt{3}(L_x^2 - L_y^2)}{3}. \quad (13)$$

Note that the u and v include the virtual processes across the CEF excited quartet states, which is different from that calculated by the $L_{x,y,z}$ restricted within the t_{2g} states. It is natural to obtain these expressions in terms of \mathbf{L} for $\delta \rightarrow 0$ instead of those of the total angular momentum \mathbf{J} since $n_{xy,yz,zx}$ does not depend on the spin. We note that (u, v) possess the offdiagonal matrix elements $\pm \frac{2-\delta}{\sqrt{2}}$ between the ground states and the excited states and their magnitudes are larger than those among the ground states. This is the source of the anisotropy in the quadrupole moments and enables one to obtain ferro quadrupole moments under antiferro quadrupole orders. In Fig. 1, the full expressions, i.e., without assumption of the small $\varepsilon (= \lambda/B_4)$ are shown as a function of ε . The offdiagonal elements for u and q_u are exactly the same, while the diagonal ones differ as ε increases. For the realistic parameter regime $\varepsilon \lesssim 0.5$, the difference between the full expression and the approximated one shown in Eqs. (11) and (12) are quantitatively the same.

The finite offdiagonal elements $\pm(2-\delta)/\sqrt{2} \sim \pm\sqrt{2}$ for $\varepsilon \lesssim 0.5$ leads to a finite cubic anisotropy in the local

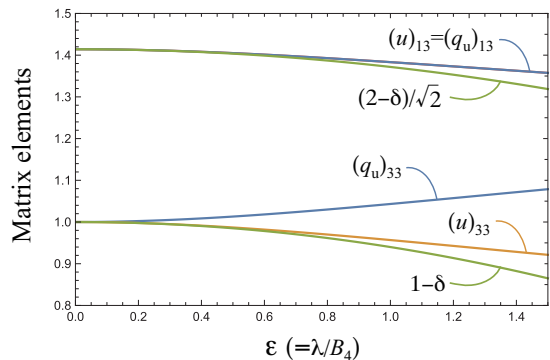


FIG. 1: The matrix elements of u and q_u as a function of $\varepsilon = \lambda/B_4$. For the offdiagonal elements, u and q_u are identical: $(u)_{13} = -(u)_{24} = (q_u)_{13} = -(q_u)_{24}$, while for the diagonal ones, they are different for finite ε :

$(u)_{33} = (u)_{44} = -(u)_{55} = -(u)_{66}$.
 $(q_u)_{33} = (q_u)_{44} = -(q_u)_{55} = -(q_u)_{66}$. The approximated values for the matrix elements of u : $1 - \delta$ and $(2 - \delta)/\sqrt{2}$, are also plotted.

quadrupole free energy, which can be calculated by the local CEF model via the Legendre transformation³⁸ as

$$F_q^{\text{loc}} \sim F_{q0}^{\text{loc}} + a(\phi_u^2 + \phi_v^2) - b(\phi_u^3 - 3\phi_u\phi_v^2) + \dots, \quad (14)$$

where F_{q0}^{loc} , a , and b are constants and ϕ_u and ϕ_v correspond to the quadrupole fields for u and v , respectively. The coefficient of the cubic anisotropy b is given by

$$b \simeq \frac{1}{2\beta^2(\frac{3}{2}\lambda)} \left(\frac{2-\delta}{\sqrt{2}} \right)^2. \quad (15)$$

Here, β is the inverse of temperature T . This is the consequence of standard Landau expansion of quadrupole free energy for $\beta\lambda \gg 1$. The T^2 dependence of b is meaningful near the quadrupolar transition temperature $T_q \simeq 33$ K and T is usually replaced by T_q for its phenomenological analysis. We note that b is proportional to the square of the offdiagonal element in u and v in Eqs. (11) and (12). The denominator $\frac{3}{2}\lambda$ represents that the perturbative processes to the CEF excited doublet are important. As for the opposite limit $\beta\lambda \sim 0$, $b \propto T$.

B. Interactions in t_{2g} manifolds

In this subsection, we introduce the exchange interactions between the t_{2g} electrons. The model used in this paper is basically given in Ref. 29, but for making this paper self-contained we summarize the model in the following.

First, we discuss exchange interactions in the quadrupole sector. We use the quadrupole-quadrupole interactions introduced in Ref. 29 with slightly different

notation^{36,37} including two parameters g_{iso} and g_{ani} as

$$H_q = \sum_{\langle i,j \rangle} (g_{\text{iso}} \mathbf{Q}_i \cdot \mathbf{Q}_j + g_{\text{ani}} \mathbf{Q}_i \cdot \mathbf{K}_{ij} \mathbf{Q}_j). \quad (16)$$

Here, $\mathbf{Q}_i \equiv (u_i, v_i)$ is the e_g quadrupole vector at the i th site and the sum runs over the nearest-neighbor sites on the fcc lattice. The bond directional anisotropic interactions are parameterized by the matrix \mathbf{K}_{ij} :

$$\mathbf{K}_{ij} = \begin{bmatrix} -1 & 0 \\ 0 & 1 \end{bmatrix} \equiv \mathbf{K}^3 \quad ij \text{ bond } \parallel xy \text{ plane}, \quad (17)$$

$$\mathbf{K}_{ij} = \begin{bmatrix} -c & s \\ s & c \end{bmatrix} \equiv \mathbf{K}^1 \quad ij \text{ bond } \parallel yz \text{ plane}, \quad (18)$$

$$\mathbf{K}_{ij} = \begin{bmatrix} -c & -s \\ -s & c \end{bmatrix} \equiv \mathbf{K}^2 \quad ij \text{ bond } \parallel zx \text{ plane}, \quad (19)$$

with $c \equiv \cos \frac{2\pi}{3}$ and $s \equiv \sin \frac{2\pi}{3}$. One can also rewrite them as

$$\mathbf{K}^n = -\hat{t}_n \hat{t}_n^T, \quad \hat{t}_n^T \equiv (\cos n\omega, \sin n\omega), \quad n = 1, 2, 3, \quad (20)$$

with $\omega \equiv 2\pi/3$. Note that the unit vector $\hat{t}_{1,2,3}$ represents the projection operator to $3x^2 - r^2$, $3y^2 - r^2$, and $3z^2 - r^2$ type orbital, respectively. The parameter V in Ref. 29 corresponds to $g_{\text{iso}} = -7V/72$ and $g_{\text{ani}} = -25V/72$. Since the ratio $g_{\text{ani}}/g_{\text{iso}} = 25/7 > 2$, this naively suggests an antiferro “ v ” order (O_{22} type) with the ordering vector at the X point: $(0, 0, 2\pi)$ from the results for E_g non-Kramers doublet systems on the fcc lattice.^{36,37} For a more general situation, the ratio $g_{\text{ani}}/g_{\text{iso}} \neq 25/7$, but in this paper we restrict ourselves to the case derived in Ref. 29 since the modification in $g_{\text{ani}}/g_{\text{iso}}$ leads to just a qualitative difference for our purpose in this paper.

For the spin part, by using the spin operator for the $\rho = xy, yz$, and zx orbital: $S_{i,\rho}^\mu \equiv \frac{1}{2} \sum_{\sigma\sigma'} d_{i,\rho\sigma}^\dagger (\hat{\sigma}^\mu)_{\sigma\sigma'} d_{i,\rho\sigma'}$, antiferromagnetic interactions are given as

$$H_{s1} = J \sum_{\langle i,j \rangle}^{xy\text{-plane}} \left(\sum_{\mu} S_{i,xy}^\mu S_{j,xy}^\mu - \frac{1}{4} n_{i,xy} n_{j,xy} \right) + (xy \rightarrow yz \text{ and } zx). \quad (21)$$

Here, $n_{i,\rho} \equiv \sum_{\sigma} d_{i,\rho\sigma}^\dagger d_{i,\rho\sigma}$ is the number operator for $\rho = xy, yz$, and zx orbitals. There are also ferromagnetic interaction,

$$H_{s2} = -J' \sum_{\langle i,j \rangle}^{xy\text{-plane}} \left[\sum_{\mu} S_{i,xy}^\mu (S_{j,yz}^\mu + S_{j,zx}^\mu) + i \leftrightarrow j \right] + \frac{3J'}{2} \sum_{\langle i,j \rangle \in xy\text{-plane}} n_{i,xy} n_{j,xy} + (xy \rightarrow yz \text{ and } zx). \quad (22)$$

$n_{i,\rho}$ is represented by the quadrupole operators as

$$n_{i,xy} = \frac{1}{3} (n_i + u_i), \quad (23)$$

$$n_{i,yz} = \frac{1}{3} \left(n_i - \frac{1}{2} u_i + \frac{\sqrt{3}}{2} v_i \right), \quad (24)$$

$$n_{i,zx} = \frac{1}{3} \left(n_i - \frac{1}{2} u_i - \frac{\sqrt{3}}{2} v_i \right), \quad (25)$$

The terms consisting of $n_{i,\rho}$'s in Eqs. (21) and (22) can be rewritten by the quadrupole forms as

$$H'_q = -\frac{J-6J'}{72} \sum_{\langle i,j \rangle} \mathbf{Q}_i \cdot (\mathbb{1} - \mathbf{K}_{ij}) \mathbf{Q}_j, \quad (26)$$

which renormalizes g_{iso} and g_{ani} in Eq. (16).

Summing up Eqs. (16), (21), and (22) with Eq. (26), we obtain the total nearest-neighbor exchange Hamiltonian as

$$H_{\text{int}} = \sum_{\langle i,j \rangle} (\tilde{g}_{\text{iso}} \mathbf{Q}_i \cdot \mathbf{Q}_j + \tilde{g}_{\text{ani}} \mathbf{Q}_i \cdot \mathbf{K}_{ij} \mathbf{Q}_j) + (J+2J') \sum_{\rho} \sum_{\langle i,j \rangle}^{\rho\text{-plane}} \mathbf{S}_{i,\rho} \cdot \mathbf{S}_{j,\rho} - J' \sum_{\rho} \sum_{\langle i,j \rangle}^{\rho\text{-plane}} (\mathbf{S}_{i,\rho} \cdot \mathbf{S}_j + \mathbf{S}_{j,\rho} \cdot \mathbf{S}_i), \quad (27)$$

where $\rho = xy, yz$, and zx . We have introduced the t_{2g} spin operators at the i site: $\mathbf{S}_i = \sum_{\rho} \mathbf{S}_{i,\rho}$ and the renormalized quadrupole interactions $\tilde{g}_{\text{iso}} = g_{\text{iso}} - \frac{1}{72}(J-6J')$ and $\tilde{g}_{\text{ani}} = g_{\text{ani}} + \frac{1}{72}(J-6J')$.

III. MEAN-FIELD RESULTS

In this section, we show the results of the mean-field analysis of the model (27) with the local part of the Hamiltonian (1). In Sec. III A, we demonstrate the results for the magnetic field $\mathbf{h} = \mathbf{0}$. For $\mathbf{h} = \mathbf{0}$, the CEF excited quartet plays just a minor role as is evident from the small factors $\delta \simeq \frac{3}{50}\epsilon^2$ and $\alpha \simeq \frac{3\sqrt{2}}{100}\epsilon^2$ in the matrix elements in the Hamiltonian (27) in addition to the energy gap $D \sim 5B_4$. See Eqs. (11), (12), and (D1)–(D3). Thus, one can consider the $\epsilon = \lambda/B_4 \rightarrow 0$ limit neglecting the CEF excited quartet states with setting $\epsilon_{3/2} = 0$, $\epsilon_{1/2} = \frac{3\lambda}{2}$, and $\epsilon'_{3/2} \simeq 5B_4 \rightarrow \infty$ in Eqs. (4), (7), and (8), respectively. Here, we shift the energy in order to set the energy of the CEF ground quartet states to 0. The matrix elements of various operators are also simplified in this limit: These simplifications are justified for $\mathbf{h} = \mathbf{0}$. In Sec. III B, we will discuss the properties under finite magnetic fields $\mathbf{h} \neq \mathbf{0}$. It turns out that one needs $O(\epsilon)$ terms in the Zeeman energy.

A. Two-sublattice mean-field approximation for zero magnetic field

Throughout this paper we assume two-sublattice orders, which are indeed observed experimentally in the double-perovskite compounds. This is because our primary purposes in this paper are to demonstrate the electronic mechanism for the induced ferro quadrupole moments under antiferro quadrupole orders (Sec. III A) and the finite magnetic moments in $J_{\text{eff}} = 3/2$ systems (Sec. III B). In recent analysis, Ref. 39 have carried out similar calculations with a four-sublattice unit cell. However, there is no comment about the finite ferro quadrupole moments in the antiferroic quadrupole phase, although the reason is unclear. For our purposes, it is sufficient to use the two-sublattice unit cell. In some parameter sets used in the following sections, the four-sublattice antiferro magnetic orders³⁹, which correspond to double- \mathbf{q} magnetic orders with induced a single- \mathbf{q} quadrupole moments, are more stabilized than FM110 states (see below), when one applies the 4-sublattice approximation. In this sense, our results within the two-sublattice orders are regarded as simple extension with the excited states from the $J_{\text{eff}} = 3/2$ model in Ref. 29. Nevertheless, the comparison between the results within the two-sublattice approximation and the experiments for the FM110 orders in Sec. III B possesses important information since regardless of which types of the microscopic interactions favor the experimentally observed FM110 phase, qualitative properties in the FM110 phase are unchanged. The detail analysis about the four-sublattice orders is one of our future problems.

Let us take the two sublattice position in the unit cell as A: $(0, 0, 0)$ and B: $(0, \frac{1}{2}, \frac{1}{2})$ and assume the ordered configurations are uniform on the xy planes: (x, y, n) and $(x + \frac{1}{2}, y, n + \frac{1}{2})$, where the lattice constant is set to unity and n is an integer and x and y represent the site positions on the $z = n$ plane. This choice corresponds to the domain with its ordering wavevector $\mathbf{k}_3^* \equiv (0, 0, 2\pi)$. The expressions for the mean-field Hamiltonian are trivially obtained and listed in Appendix C. The inclusion of the CEF excited doublet in the model Hamiltonian causes only small effects on the overall feature of the phase diagram and the magnitude of the primary order parameters. Thus, the qualitative results here are almost identical to those in Ref. 29 except for the ferroic quadrupole moments.

Figure 2 shows the temperature dependence of the ferro and antiferro quadrupole moments defined as

$$\mathbf{Q}^{\text{F}} \equiv \langle \mathbf{Q} \rangle_{\text{A}} + \langle \mathbf{Q} \rangle_{\text{B}}, \quad \mathbf{Q}^{\text{AF}} \equiv \langle \mathbf{Q} \rangle_{\text{A}} - \langle \mathbf{Q} \rangle_{\text{B}}. \quad (28)$$

Here $\langle \cdot \rangle_{\text{A(B)}}$ indicates the expectation value calculated by the A(B)-site local mean-field Hamiltonian. The data for $\lambda/J = 10^4 \gg 1$ corresponds to those shown in Fig. 8 in Ref. 29. For these parameter sets, the system undergoes a phase transition into a pure quadrupolar phase with the primary antiferroic and induced ferroic ones (AFQ+ f q) at $T/J \simeq 0.9$ and another transition at $T/J \simeq 0.3$ into

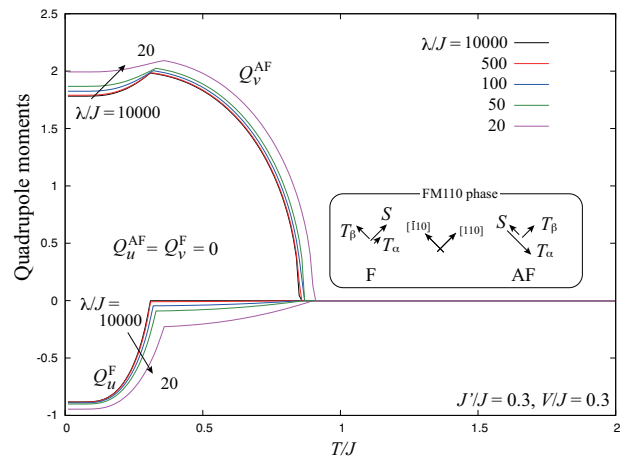


FIG. 2: Temperature dependence of the quadrupole moments Q_u^{F} and Q_v^{AF} for $J'/J = 0.3$, $V/J = 0.3$, and $\lambda/J = 10^4$, 500, 100, 50, and 20. $Q_v^{\text{F}} = Q_u^{\text{AF}} = 0$ and are not shown.

a magnetic phase (FM110). The order parameter configuration of the FM110 phase is schematically shown in Fig. 2: the x and y components of the ferro/antiferro dipole $\mathbf{S}^{\text{F,AF}}$ and ferro/antiferro octupole $\mathbf{T}_{\alpha,\beta}^{\text{F,AF}}$ moments take finite values. The definition of these multipole moments are given in Appendix B and we use the definition of “F/AF” similarly to Eq. (28). Note that the realistic value of λ in Fig. 2 is e.g., $\lambda/J = 100$ barring the magnetic transition temperature ~ 20 K in mind. One can see a finite $Q_u^{\text{F}} \lesssim -0.1$ inside the AFQ+ f q phase for $0.3 \lesssim T/J \lesssim 0.9$. It is quite natural that as λ decreases and thus the energy of the excited doublet $\epsilon_{1/2}$ lowers, the ferro moment $|Q_u^{\text{F}}|$ increases. It is interesting that the effect of the excited state is not negligible even if the excited state energy is 100 times larger than the transition temperature into the quadrupole order. The presence of the excited doublet also affects the transition temperatures and the two transition temperatures slightly increase upon decreasing λ but these are minor points.

Figure 3 shows T - λ phase diagram for $V/J = 0.3$ and $J'/J = 0.1$ – 0.5 . For these parameter sets, the AFQ+ f q phase robustly appears from the normal (paramagnetic) state via the second-order transition. For $J'/J = 0.3$ and 0.5 , the ground state is the FM110, whose configuration is shown in the inset of Fig. 2. For $J'/J = 0.1$, the ground states change with varying λ . When λ is large, the planer antiferromagnetic (AFM) order takes place, where $S_y^{\text{AF}}/S_x^{\text{AF}} = T_{\alpha,y}^{\text{AF}}/T_{\alpha,x}^{\text{AF}} = -T_{\beta,y}^{\text{AF}}/T_{\beta,x}^{\text{AF}}$ and the other multipole moments are zero. As noted in Ref. 29, owing to an accidental degeneracy there is no anisotropy and $S_{x,y}^{\text{AF}} = 0$ at $T = 0$, while the x and y components of $\mathbf{T}_{\alpha,\beta}^{\text{AF}}$ are finite. This feature continues even for finite λ . This is because the ground-state wavefunction at each sublattice (A and B) in the AFM phase for finite λ is ex-

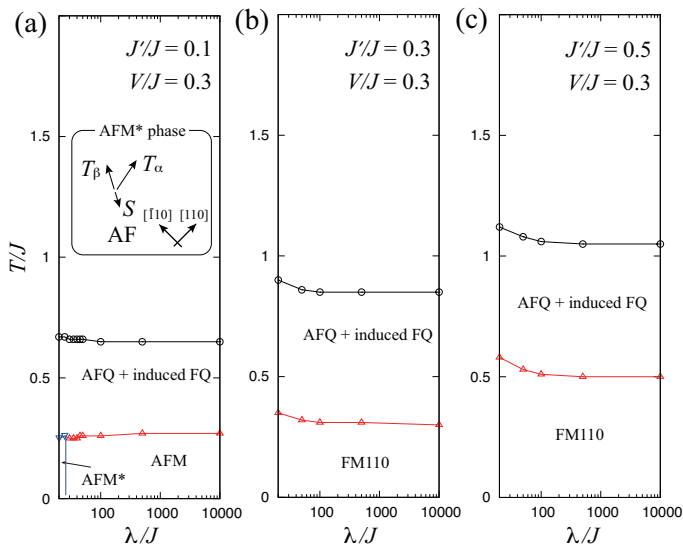


FIG. 3: T - λ phase diagram for $V/J = 0.3$, and (a) $J'/J = 0.1$, (b) 0.3 , and (c) 0.5 . Inset in (a): the antiferromagnetic configurations \mathbf{S}^{AF} , $\mathbf{T}_\alpha^{\text{AF}}$, and $\mathbf{T}_\beta^{\text{AF}}$ in the AFM* phase.

actly the same as that at $\lambda = \infty$, which is the eigenstate of the quadrupole moment $\langle \mathbf{Q} \rangle_{A,B} = (-1 + \delta, 0)$. As is evident from Eq. (11), the matrix u does not have finite matrix elements between the excited states and the fifth and sixth states, while v in Eq. (12) does. In the language of \mathbf{S}_ρ , the ground state is characterized by $\langle \mathbf{S}_{xy} \rangle_{A,B} = \mathbf{0}$, $\langle S_{yz, zx}^z \rangle_{A,B} = 0$, $\langle S_{yz}^\mu \rangle_A = -\langle S_{yz}^\mu \rangle_B = -\langle S_{zx}^\mu \rangle_A = \langle S_{zx}^\mu \rangle_B$ with $\mu = x$ or y . They ensure that the state with $\langle \mathbf{Q} \rangle_{A,B} = (-1 + \delta, 0)$ remains to be decoupled from the excited states since there is only a term proportional to $S_{i,yz}^\mu - S_{i,zx}^\mu$ ($\mu = x, y$) in the magnetic sector of the mean-field Hamiltonian at the site i . See Appendix C. This has indeed no matrix element between the states with $u = -1 + \delta$ and the excited states as in u . See their expressions in Eqs. (D7), (D8), (D10), and (D11).

In contrast, for small λ , the low- T phase is another antiferromagnetic phase (AFM*) as schematically shown in the inset of Fig. 3(a). The order parameters for the AFM* phase are similar to those in the AFM phase, but there are finite $S_{x,y}^{\text{AF}}$ moments even at $T = 0$. To realize the AFM* phase, the spin-orbit coupling λ is tuned to be $\lambda \lesssim 30J$, where a finite quadrupole moments v appears and thus the symmetry is lowered. This also causes a finite mixing between the states with $u = -1 + \delta$ and the excited states. Thus, the ground-state wavefunction in the AFM state is no longer eigen state of the mean-field Hamiltonian. Then, a different state becomes the ground state with a finite \mathbf{S}^{AF} . Indeed, such transition has been studied in the non-Kramers Γ_3 system in our previous study³⁷, where a kind of topological protection is important. However, the value of the spin-orbit coupling is not realistic, and thus, we do not analyze it in detail here.

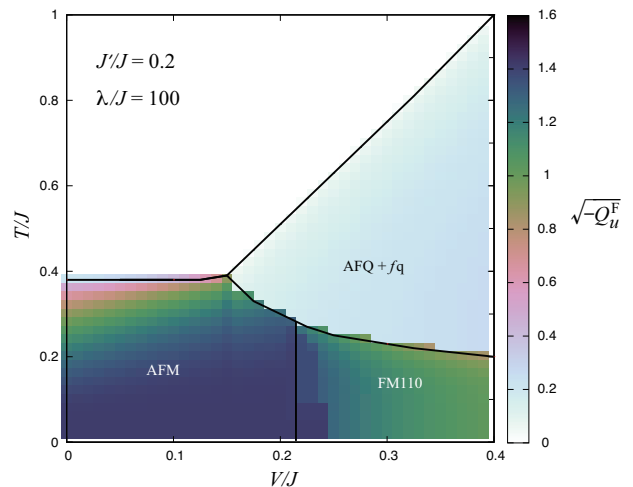


FIG. 4: T - V phase diagram for $J'/J = 0.2$. The lines represent the phase boundaries. The color map shows $\sqrt{-Q_u^F}$, where $Q_u^F \leq 0$ for any V and T . The square-root of $-Q_u^F$ is used just for visualization of the small value of Q_u^F in the AFQ phase.

Let us now examine the T - V phase diagram for the realistic value of $\lambda \simeq 100J$. There are three phases: the AFM, the AFQ+ f_q , and the FM110 phases in Fig. 4. For visualizing the magnitude of the Q_u^F in the ordered phases, $\sqrt{-Q_u^F}$ is also depicted in Fig. 4 as colormap. The reason for using the “square-root” is just due to the technical one to show the finiteness in the AFQ+ f_q phase, where the $|Q_u^F|$ is much smaller than that in the other ordered phases. We have checked that even for $\lambda/J = 10000$ ignoring the excited states, the phase diagram is semiquantitatively the same as that shown in Fig. 4. The difference is that the $Q_u^F \simeq 0$ in the AFQ+ f_q for $\lambda/J = 10000$, which corresponds to the results in Ref. 29.

B. Finite magnetic fields

Under the magnetic field $\mathbf{h} = (h_x, h_y, h_z)$, which includes the Bohr magneton μ_B and is related to the real magnetic field \mathbf{H} as $\mathbf{h} = \mu_B \mathbf{H}$, we introduce the Zeeman coupling with the electronic g factor with $g = 2$ as

$$H_Z = - \sum_{\sigma, \sigma', m, m'} \mathbf{h} \cdot (\mathbf{M})_{\sigma\sigma', mm'} d_{m\sigma}^\dagger d_{m'\sigma'}. \quad (29)$$

Here, the magnetic moment operator is defined as $(\mathbf{M})_{\sigma\sigma', mm'} \equiv [(\mathbb{1})_{\sigma\sigma'} (\mathbf{L})_{mm'} + 2\mathbf{s}_{\sigma\sigma'} (\mathbb{1})_{mm'}]$. In actual calculations for the six states manifold, \mathbf{M} reduces to the matrix form listed in Eqs. (D1)–(D3) and Eqs. (D13)–(D15).

To determine which ordering wavevectors are stabilized under the magnetic fields within the two-sublattice mean-field approximation, we repeat the calculations with dif-

ferent ordering wavevector set up: $\mathbf{k}_1^* = (2\pi, 0, 0)$, $\mathbf{k}_2^* = (0, 2\pi, 0)$, and $\mathbf{k}_3^* = (0, 0, 2\pi)$ and compare their free energies. We note that the diagonal matrix elements of \mathbf{M} in the bases of the eigenstates of the Hamiltonian (1) are $O(\varepsilon)$ in the CEF ground-state quartet. For example, the diagonal elements of M_z is $\text{diag}(1, -1, \frac{4}{5}\varepsilon + \frac{1}{50}\varepsilon^2, -\frac{4}{5}\varepsilon - \frac{1}{50}\varepsilon^2, 0, 0) + O(\varepsilon^3)$. Thus, the half of the quartet state with $u \simeq 1$ has a finite dipole moment $\sim \frac{4}{5}\varepsilon\mu_B \simeq 0.4\mu_B$, which has not been recognized well so far.

Before discussing the numerical data, we should note the followings. Using the $O(\varepsilon)$ terms in the \mathbf{M} means that we treat the CEF ground state quartet as *effective* t_{2g} state with hybridizing to the excited quartet. This treatment is valid if the interaction (27) are not modified significantly when the processes related to the e_g electrons are also taken account. In this study, we do not estimate such processes and we keep the interaction form derived within the t_{2g} states as a starting approximation. The more sophisticated analysis remains as one of our future problems.

Figure 5 shows the magnetization $M_h \equiv \langle \mathbf{M} \rangle \cdot \mathbf{h}/h$ and $|\langle \mathbf{M} \rangle|$ for $J'/J = 0.3$ and $V/J = 0.27$ as a function of $h = |\mathbf{h}|$ for three high-symmetric directions $\mathbf{h} \parallel [001]$, $[110]$, and $[111]$. At $h = 0$, the ground state is the FM110 phase and the intermediate-temperature phase is the AFQ+ f q phase for this parameter set. As for the scale of the magnetic field, $h/J = 0.1$ corresponds to ~ 10 T if we set the magnetic transition temperature $T_m \sim 0.34J \sim 20$ K. There are three equivalent domains for the FM110-type phases: FM110, FM101, and FM011. As can be trivially understood, these phases have its magnetization along $[110]$, $[101]$, and $[011]$ directions, respectively. A finite magnetic field selects some of the three domains and the results are shown only for those with the lowest free energy.

Owing to the difference in the field direction and that for the spontaneous one for $\mathbf{h} \parallel [001]$ and $[111]$, $M \neq M_h$, while $M = M_h$ for $\mathbf{h} \parallel [110]$. One can notice that the increase in M_h as increasing h is steepest for $\mathbf{h} \parallel [001]$. This is related to the fact that the ferro quadrupole moment Q_u^F is large in the FM110 phase (Fig. 2) and the increase in $M_h = M_z$ is more favored than that for $\mathbf{h} \parallel [111]$. In the AFQ+ f q phase, the magnetic field also selects the two of the domains: \mathbf{k}_1 or \mathbf{k}_2 . However, the energy difference between the domains with $\mathbf{k}_{1,2}$ and \mathbf{k}_3 is so tiny and it is not physically important in actual situations, where there are many aspects such as electron-lattice couplings.

IV. DISCUSSIONS

In the following subsections, we discuss two aspects. The first is the induced ferro quadrupole moments under the antiferro quadrupole orders. The second is the magnitude of the magnetic moment, which vanishes in the model of $J_{\text{eff}} = 3/2$.

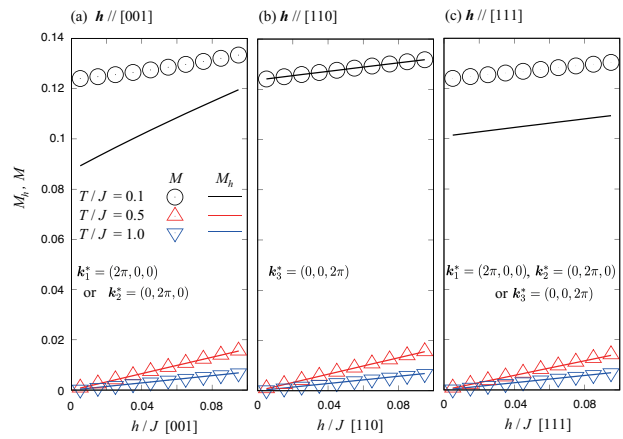


FIG. 5: Magnetization curve for $J'/J = 0.3$ and $V/J = 0.27$. (a) $\mathbf{h} \parallel [001]$, (b) $\mathbf{h} \parallel [110]$, and (c) $\mathbf{h} \parallel [111]$. The magnetization M_h is defined as $M_h \equiv \langle \mathbf{M} \rangle \cdot \mathbf{h}/h$, with $h \equiv |\mathbf{h}|$ and plotted by lines, while the absolute value $M \equiv |\langle \mathbf{M} \rangle|$ is indicated by symbols. The domain with the lowest free energy is considered; (a) \mathbf{k}_1 or \mathbf{k}_2 domains, (b) \mathbf{k}_3 domain, and (c) \mathbf{k}_1 , \mathbf{k}_2 , or \mathbf{k}_3 domains. The temperatures shown correspond to the FM110 phase ($T/J = 0.1 < T_m/J \simeq 0.34$), the AFQ+ f q phase ($T/J = 0.5$), and the normal phase ($T/J = 1.0$).

A. Ferro quadrupole moments

Let us compare the results in Sec. III and the experimental data in the double perovskite compound focusing on the ferro quadrupole moments observed in $\text{Ba}_2\text{MgReO}_6$ ³¹. The relative magnitude of the antiferro quadrupole Q_v^{AF} and the ferro quadrupole Q_u^{F} moments can be indirectly estimated by observing O displacement ($\varepsilon_u, \varepsilon_v$) corresponding to (u, v) in the ordered phases. At $T = 6$ K, i.e., inside the magnetically-ordered phase, Hirai et al., reported that there is about 0.4 % elongation of the oxygen octahedron along the $z(c)$ axis in average. Here “average” means that the analysis without inplane v type displacement. With the further analysis including this inplane displacements, they estimated that the ratio $v/u \sim Q_v^{\text{AF}}/Q_u^{\text{F}} \sim 4$. Here, we have assumed a linear relation between the oxygen displacement and the d -electron quadrupole moments, ignoring anharmonic couplings. In the Supplemental Material in Ref. 31, the data of average oxygen positions at $T = 25$ K inside the quadrupolar phase are also listed. One can estimate 0.18 % elongation of the oxygen octahedron along the $z(c)$ axis in average. This naively leads to the ratio $Q_v^{\text{AF}}/Q_u^{\text{F}} \sim 8$. Although there is ambiguity about the quadrupole-displacement coupling, which can be anisotropic even in the first-order in $Q_{u,v}$, the finite values of Q_u^{F} shown in Fig. 2 are qualitatively consistent with this. Indeed, when setting $J \sim 50$ K and $\lambda/J = 50\text{--}100$, the AFQ order appears at $T_q \sim 40$ K and

the magnetic one at $T_m \sim 25$ K in Fig. 2. In actual situation, one should take into account couplings between the electrons and the oxygen displacement as discussed recently^{32,40}. Nevertheless, this result demonstrates that the contribution of the excited states on the induced ferro quadrupole moments in the AFQ state is a noticeable in the double perovskite materials.

B. Effective magnetic moment

We now discuss the magnetic properties of this system. It is well known that the magnetic moment \mathbf{M} in the effective $J_{\text{eff}} = 3/2$ theory, i.e., $\varepsilon \rightarrow 0$ limit, vanishes. This is one of the weak points in the theory and some discussions about the impact of the orbital orders on the magnetic susceptibility have been done recently³⁹. Let us estimate the effective moment μ_{eff} defined by the high-temperature asymptotic form of the magnetic susceptibility as

$$\mu_B M_z \simeq \mu_B \frac{\frac{4\varepsilon}{5}(e^{\frac{4}{5}\varepsilon h/T} - e^{-\frac{4}{5}\varepsilon h/T})}{e^{\frac{4}{5}\varepsilon h/T} + e^{-\frac{4}{5}\varepsilon h/T} + 2} \simeq \frac{(\frac{\sqrt{3}}{\sqrt{2}}\frac{4}{5}\varepsilon\mu_B)^2}{3T} \frac{h}{\mu_B}, \quad (30)$$

where we have assumed $\mathbf{h} \parallel [001]$. Thus,

$$\mu_{\text{eff}} = \frac{4\sqrt{3}}{5\sqrt{2}}\varepsilon\mu_B = \frac{4\sqrt{2}}{\sqrt{3}} \left(\frac{\frac{3}{2}\lambda}{5B_4} \right) \mu_B. \quad (31)$$

As is evident from the factor $\frac{3}{2}\lambda/(5B_4)$, this arises from the hybridization between the ground and excited quartets. Remember that the induced ferro quadrupole moments discussed in the previous subsection arises from the offdiagonal elements of the quadrupole operators between the ground state quartet and the first excited doublet. Substituting the values for Rb_2TaCl_6 with $D \simeq 5B_4 \simeq 3.2$ eV and $\lambda \simeq 0.27$ eV leading to $\varepsilon \simeq 0.42$, the effective moment is estimated as $\mu_B \simeq 0.41\mu_B$, which is similar to the observed one $0.27\mu_B$ ²³. When using the typical values for the double-perovskites, $3\lambda/2 \sim 0.5$ eV^{24,28} and $D \sim 5$ eV²⁵, one finds $\mu_{\text{eff}} \simeq 0.49\mu_B$. The present estimation is not far from the observed one $\mu_{\text{eff}} \simeq 0.68\mu_B$ ²² in $\text{Ba}_2\text{MgReO}_6$. The remaining discrepancy might be improved by taking into account the effects of ligand ions²⁸ and/or the vibronic degrees of freedom³². The fluctuation effects neglected in the present analysis also affect the magnitude of the magnetic moment quantitatively. Analyses including these more sophisticated aspects are one of our future problems.

Compared to the estimation of μ_{eff} , the results of the ordered magnetic moment shown in Fig. 5 is not satisfactory in the present mean-field analysis. As discussed in Fig. 5, which roughly corresponds to the parameter set for $\text{Ba}_2\text{MgReO}_6$ with setting $J \sim 50$ K, M_h and M are ~ 0.1 . This is only ~ 20 – 30 % of the observed moment in $\text{Ba}_2\text{MgReO}_6$ ²². As shown in Fig. 2, $Q_u^F < 0$ and this corresponds to larger occupation in the yz and zx orbitals at $h = 0$. In terms of the four states in the ground state

quartet, the energy of the \downarrow states ($J_{\text{eff}}^z = \pm 3/2$) is lower than that for the \uparrow states ($J_{\text{eff}}^z = \pm 1/2$). See Eqs. (A3)–(A6) and the matrix u in Eq. (11). The point is that these \downarrow states have no moment even with the $O(\varepsilon^2)$ correction. Thus, the ordered moment is smaller compared with the effective moment even without the additional $\sqrt{3}$ factor in the definition of μ_{eff} : $0.49/\sqrt{3} = 0.28 > 0.1$. Recently, Zhang et al., have proposed that the quadrupole configurations in the AFQ+ f q phase modifies the spin-spin exchange interactions and the Dzyaloshinskii-Moriya type interaction induced in the AFQ+ f q phase stabilizes the magnetic order of FM110 and obtained a reasonable value of the ferro moments,⁴¹ although the relation between the CEF excited quartet states are not clear.

In Ref. 28, the orbital angular momentum renormalization was discussed. Owing to the extended d like orbital including the surrounding p orbitals at the oxygen sites, $\mathbf{M} = 2\mathbf{S} + \mathbf{L} \rightarrow 2\mathbf{S} + \gamma\mathbf{L}$ with $\gamma = 0.536$ for $\text{Ba}_2\text{MgReO}_6$. Although it is unclear whether their analysis without the cubic anisotropy includes the effect of the local excited states shown in this paper, let us here qualitatively examine how this renormalization effect influences the results in our model. By introducing γ in Eq. (29), the value of M and M_h change as decreasing γ from $\gamma = 1$. For the parameters shown in Fig. 5, firstly M and M_h decrease and vanish at $\gamma \sim 0.8$ and then increase. At $\gamma = 0.5$, $M_h \sim 0.25$ as shown in Fig. 6. In actual situation in real materials, not only the Zeeman energy (29), but also the interactions (27) must be modified. Nevertheless, a finite ε modifies the orbital character in the presence of the renormalization owing to γ . As shown in Fig. 6, the orbital contributing to the magnetic moment is $\sim \uparrow$ state ($J_{\text{eff}}^z = \pm 1/2$) for $\gamma \sim 1$, while \downarrow components ($J_{\text{eff}}^z = \pm 3/2$) increase as lowering γ . For the ferro quadrupolar phase observed in Rb_2TaCl_6 and Cs_2TaCl_6 , $Q_u^F > 0$ and $\gamma \sim 0.8$ is estimated²³. Since $Q_u^F > 0$, \uparrow components (i.e., $J_{\text{eff}} = \pm 1/2$) are energetically favored both by the uniform distortions and magnetic fields.

For smaller γ , the correction owing to the excited state proportional to ε is minor in the present simplified analysis. However, for large ε , $\mu_{\text{eff}} \sim 0.5\mu_B$ without the correction owing to the ligand ions. It is expected that the combined corrections by the excited states and the ligand ions influence the orbital character of the magnetic moment in more complex ways than discussed here. The theory describing the magnetic moment in the $J_{\text{eff}} = 3/2$ model requires more elaborate treatments and the interpretation of the experimental results should also be reconsidered. In this respect, it is highly important to clarify the orbital profile, i.e., the ratio between \uparrow and \downarrow , of the magnetic moments as analyzed in, e.g., LiV_2O_4 ⁴².

V. SUMMARY

We have clarified that the ferroic components of O_{20} are induced under the antiferroic O_{22} orders in the fcc lattice model. We have microscopically demonstrated the

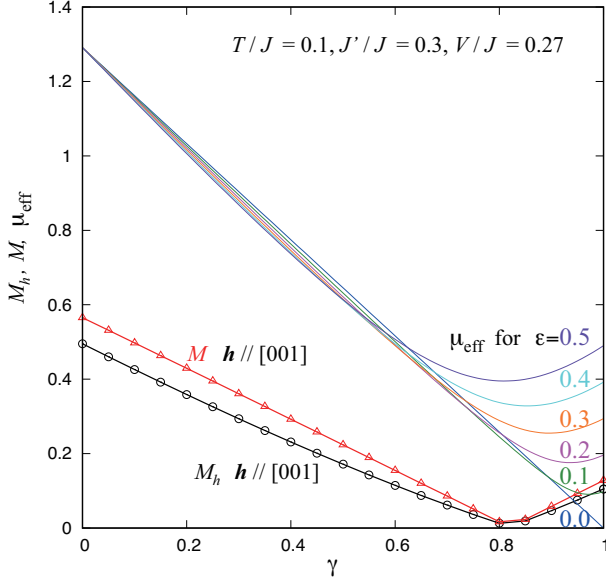


FIG. 6: γ dependence of M , M_h for $T/J = 0.1$ K, $h/J = 0.05$ along $\mathbf{h} \parallel [001]$, $J'/J = 0.3$ and $V/J = 0.27$. The effective moment μ_{eff} 's given by Eq. (31) for several values of ε are also drawn.

mechanism of the induced ferroic moments. This is in fact quite simple: just taking into account the CEF excited doublet state. It is important that the excited state located at ~ 5000 K, ~ 100 times larger scale than the transition temperature $T_q \sim 30$ K, can influence the order parameter via generating the local anisotropy. We have also clarified that the magnetic dipole moment in the $J_{\text{eff}} = 3/2$ model does not vanish in the realistic values of the spin-orbit coupling and crystalline electric field, when the CEF excited quartet states are taken into account. Since these aspects have not been seriously considered so far, we believe our results shed a renewed light on the orbital orders in related correlated systems.

ACKNOWLEDGMENT

This work was supported by JSPS KAKENHI (Grant No. JP21H01031 and No. JP23H04869).

Appendix A: Wavefunctions

We list the lowest 6 local eigenstates for $\lambda > 0$ and $B_4 > 0$. They are mainly constructed by the t_{2g} orbitals in the parameter regime relevant to our considerations. In terms of $m\sigma$ bases $\{2 \uparrow, 1 \uparrow, 0 \uparrow, -1 \uparrow, -2 \uparrow, 2 \downarrow, 1 \downarrow, 0 \downarrow, -1 \downarrow, -2 \downarrow\}$, the local eigenstates for the Γ_7 with the energy $\epsilon_{1/2}$ and the Γ_8 with $\epsilon_{3/2}$ are expressed as

$$|\Gamma_7+\rangle : \{0, -2, 0, 0, 0, -1, 0, 0, 0, 1\}, \quad (\text{A1})$$

$$|\Gamma_7-\rangle : \{-1, 0, 0, 0, 1, 0, 0, 0, 2, 0\}, \quad (\text{A2})$$

$$|\Gamma_8+\uparrow\rangle : \left\{0, \frac{\varepsilon}{4} + \frac{w}{4} + \frac{1}{2}, 0, 0, 0, -\frac{\varepsilon}{2} - \frac{w}{2}, 0, 0, 0, 1\right\}, \quad (\text{A3})$$

$$|\Gamma_8-\uparrow\rangle : \left\{1, 0, 0, 0, -\frac{\varepsilon}{2} - \frac{w}{2}, 0, 0, 0, \frac{\varepsilon}{4} + \frac{w}{4} + \frac{1}{2}, 0\right\}, \quad (\text{A4})$$

$$|\Gamma_8-\downarrow\rangle : \left\{0, 0, 0, -1 - \frac{\varepsilon}{10} - \frac{w}{2}, 0, 0, 0, \frac{\sqrt{6}}{5}\varepsilon, 0, 0\right\}, \quad (\text{A5})$$

$$|\Gamma_8+\downarrow\rangle : \left\{0, 0, \frac{\sqrt{6}}{5}\varepsilon, 0, 0, 0, -1 - \frac{\varepsilon}{10} - \frac{w}{2}, 0, 0, 0\right\}, \quad (\text{A6})$$

where we have not normalized the eigenstates and $w \equiv \sqrt{\varepsilon^2 + 4\varepsilon/5 + 4}$. We have labeled these states by the diagonal matrix elements of J_z and u for $\varepsilon \rightarrow 0$. The label \pm represents the sign of the diagonal matrix element J_z in Eq. (9), while the quadrupole part \uparrow (\downarrow) in the Γ_8 states indicates the positive (negative) diagonal matrix element u in Eq. (11).

Appendix B: Multipole operators

We here list various multipole operators appearing in the Hamiltonian (27). In the following, we omit the site index i for simplicity.

$$S_{xy}^\mu = \frac{1}{3} \left[\frac{1}{2} \hat{\sigma}^\mu + \frac{1}{2} \hat{\sigma}^\mu \hat{u} \right], \quad (\text{B1})$$

$$S_{yz}^\mu = \frac{1}{3} \left[\frac{1}{2} \hat{\sigma}^\mu + \frac{1}{2} \hat{\sigma}^\mu \left(-\frac{1}{2} \hat{u} + \frac{\sqrt{3}}{2} \hat{v} \right) \right], \quad (\text{B2})$$

$$S_{zx}^\mu = \frac{1}{3} \left[\frac{1}{2} \hat{\sigma}^\mu + \frac{1}{2} \hat{\sigma}^\mu \left(-\frac{1}{2} \hat{u} - \frac{\sqrt{3}}{2} \hat{v} \right) \right]. \quad (\text{B3})$$

Here, $\hat{\sigma}^\mu/2$ represents the spin operator of the t_{2g} orbital: $S_{xy}^\mu + S_{yz}^\mu + S_{zx}^\mu$, and $\frac{1}{2} \hat{\sigma}^\mu \hat{u}$ and $\frac{1}{2} \hat{\sigma}^\mu \hat{v}$ are the spin-orbital composite ones: $2S_{xy}^\mu - S_{yz}^\mu - S_{zx}^\mu$ and $\sqrt{3}(S_{yz}^\mu - S_{zx}^\mu)$, respectively. In terms of the irreducible representation of the O_h group, the operators belonging to Γ_4 are

$$\mathbf{S} \equiv \frac{1}{2} \{ \hat{\sigma}^x, \hat{\sigma}^y, \hat{\sigma}^z \}, \quad (\text{B4})$$

$$\mathbf{T}_\alpha \equiv \frac{1}{2} \left\{ \hat{\sigma}^x \left(-\frac{1}{2} \hat{u} + \frac{\sqrt{3}}{2} \hat{v} \right), \hat{\sigma}^y \left(-\frac{1}{2} \hat{u} - \frac{\sqrt{3}}{2} \hat{v} \right), \hat{\sigma}^z \hat{u} \right\}, \quad (\text{B5})$$

and those belonging to Γ_5 are

$$\mathbf{T}_\beta \equiv \frac{1}{2} \left\{ \hat{\sigma}^x \left(-\frac{\sqrt{3}}{2} \hat{u} - \frac{1}{2} \hat{v} \right), \hat{\sigma}^y \left(\frac{\sqrt{3}}{2} \hat{u} - \frac{1}{2} \hat{v} \right), \hat{\sigma}^z \hat{v} \right\}. \quad (\text{B6})$$

Using these irreps., one finds

$$S_{xy}^x = \frac{1}{3} \left[S^x - \frac{1}{2} T_\alpha^x - \frac{\sqrt{3}}{2} T_\beta^x \right], \quad (\text{B7})$$

$$S_{xy}^y = \frac{1}{3} \left[S^y - \frac{1}{2} T_\alpha^y + \frac{\sqrt{3}}{2} T_\beta^y \right], \quad (\text{B8})$$

$$S_{xy}^z = \frac{1}{3} (S^z + T_\alpha^z), \quad (\text{B9})$$

$$S_{yz}^x = \frac{1}{3} (S^x + T_\alpha^x), \quad (\text{B10})$$

$$S_{yz}^y = \frac{1}{3} \left[S^y - \frac{1}{2} T_\alpha^y - \frac{\sqrt{3}}{2} T_\beta^y \right], \quad (\text{B11})$$

$$S_{yz}^z = \frac{1}{3} \left[S^z - \frac{1}{2} T_\alpha^z + \frac{\sqrt{3}}{2} T_\beta^z \right], \quad (\text{B12})$$

$$S_{zx}^x = \frac{1}{3} \left[S^x - \frac{1}{2} T_\alpha^x + \frac{\sqrt{3}}{2} T_\beta^x \right], \quad (\text{B13})$$

$$S_{zx}^y = \frac{1}{3} (S^y + T_\alpha^y), \quad (\text{B14})$$

$$S_{zx}^z = \frac{1}{3} \left[S^z - \frac{1}{2} T_\alpha^z - \frac{\sqrt{3}}{2} T_\beta^z \right]. \quad (\text{B15})$$

Appendix C: Mean-field Hamiltonian

We show the detail expression of the two-site mean-field Hamiltonian used in the maintext. The total mean-field Hamiltonian is $H_{\text{int}}^{\text{mf}} = H_{\text{int}}^{\text{A}} + H_{\text{int}}^{\text{B}} + C$, where $H_{\text{int}}^{\text{A(B)}}$ is the mean-field Hamiltonian at the A(B) sublattice and C is a constant depending on the order parameters. Denoting the expectation values of order parameters X at the A(B) sublattice as $\langle X \rangle_{\text{A(B)}}$, we obtain $H_{\text{int}}^{\text{A}} = \sum_{i \in \text{A}} (H_{\text{int},i}^{\text{A},xy} + H_{\text{int},i}^{\text{A},yz} + H_{\text{int},i}^{\text{A},zx})$, where

$$H_{\text{int},i}^{\text{A},xy} = z_{\text{nn}} \left\{ \langle \mathbf{Q} \rangle_{\text{A}} \cdot \left(\tilde{g}_{\text{iso}} \mathbb{1} + \tilde{g}_{\text{ani}} \mathbf{K}^3 \right) \mathbf{Q}_i - J' \langle \mathbf{S}_{xy} \rangle_{\text{A}} \cdot \mathbf{S}_i + \left[(J + 2J') \langle \mathbf{S}_{xy} \rangle_{\text{A}} - J' \langle \mathbf{S} \rangle_{\text{A}} \right] \cdot \mathbf{S}_{i,xy} \right\}, \quad (\text{C1})$$

$$H_{\text{int},i}^{\text{A},yz} = z_{\text{nn}} \left\{ \langle \mathbf{Q} \rangle_{\text{B}} \cdot \left(\tilde{g}_{\text{iso}} \mathbb{1} + \tilde{g}_{\text{ani}} \mathbf{K}^1 \right) \mathbf{Q}_i - J' \langle \mathbf{S}_{yz} \rangle_{\text{B}} \cdot \mathbf{S}_i + \left[(J + 2J') \langle \mathbf{S}_{yz} \rangle_{\text{B}} - J' \langle \mathbf{S} \rangle_{\text{B}} \right] \cdot \mathbf{S}_{i,yz} \right\}, \quad (\text{C2})$$

where i obviously belongs to the A sublattice sites and $z_{\text{nn}} = 4$ is the number of the nearest neighbor sites on each of the xy, yz , and zx plane. Similarly to $H_{\text{int},i}^{\text{A},yz}$, $H_{\text{int},i}^{\text{A},zx}$ can be obtained by replacing $yz \rightarrow zx$ and $\mathbf{K}^1 \rightarrow \mathbf{K}^2$ in Eq. (C2). The mean-field Hamiltonian at the B sublattice $H_{\text{int}}^{\text{B}}$ is also trivially obtained by replacing $\text{A} \leftrightarrow \text{B}$ in Eqs. (C1) and (C2). The constant part C is necessary for calculating the free energy and this is given as

$$\frac{C}{z_{\text{nn}} N} = \sum_{\alpha=\text{A,B}} \left[- \langle \mathbf{Q} \rangle_{\alpha} \frac{\tilde{g}_{\text{iso}} \mathbb{1} + \tilde{g}_{\text{ani}} \mathbf{K}^3}{2} \cdot \langle \mathbf{Q} \rangle_{\alpha} + J' \langle \mathbf{S}_{xy} \rangle_{\alpha} \cdot \langle \mathbf{S} \rangle_{\alpha} - \frac{J + 2J'}{2} |\langle \mathbf{S}_{xy} \rangle_{\alpha}|^2 \right] + \left[- \langle \mathbf{Q} \rangle_{\text{A}} \left(\tilde{g}_{\text{iso}} \mathbb{1} + \tilde{g}_{\text{ani}} \mathbf{K}^1 \right) \cdot \langle \mathbf{Q} \rangle_{\text{B}} + J' \left(\langle \mathbf{S}_{yz} \rangle_{\text{A}} \cdot \langle \mathbf{S} \rangle_{\text{B}} + \langle \mathbf{S} \rangle_{\text{A}} \cdot \langle \mathbf{S}_{yz} \rangle_{\text{B}} \right) - (J + 2J') \langle \mathbf{S}_{yz} \rangle_{\text{A}} \cdot \langle \mathbf{S}_{yz} \rangle_{\text{B}} + (yz \rightarrow zx) \right]. \quad (\text{C3})$$

Note that N is the number of the unit cell (= the number of the A sublattice) and remember $\mathbf{K}^1 \rightarrow \mathbf{K}^2$ when $yz \rightarrow zx$.

Appendix D: Matrix form of multipole operators

The explicit 6×6 matrix forms of the spin and angular momentum operators are listed below. First, the spin operators \mathbf{S} 's are given with $\alpha = \frac{3\sqrt{2}}{100} \varepsilon^2 + O(\varepsilon^3) \simeq \sqrt{2} \delta$ in Eq. (11) as,

$$S^x \simeq \frac{1}{6} \begin{bmatrix} 0 & 1 & 0 & -\sqrt{2} + \alpha & 0 & -\sqrt{6} + \sqrt{3}\alpha \\ 0 & \sqrt{2} - \alpha & 0 & 0 & -\sqrt{6} + \sqrt{3}\alpha & 0 \\ 0 & 0 & -2 + 2\sqrt{2}\alpha & 0 & 0 & \sqrt{3} - \sqrt{6}\alpha \\ 0 & 0 & 0 & -\sqrt{3} + \sqrt{6}\alpha & 0 & 0 \\ 0 & 0 & 0 & 0 & 0 & 0 \\ 0 & 0 & 0 & 0 & 0 & 0 \end{bmatrix}, \quad (\text{D1})$$

$$S^y \simeq \frac{i}{6} \begin{bmatrix} 0 & 1 & 0 & -\sqrt{2} + \alpha & 0 & \sqrt{6} - \sqrt{3}\alpha \\ 0 & -\sqrt{2} + \alpha & 0 & 0 & -\sqrt{6} + \sqrt{3}\alpha & 0 \\ 0 & 0 & -2 + 2\sqrt{2}\alpha & 0 & 0 & -\sqrt{3} + \sqrt{6}\alpha \\ 0 & 0 & 0 & -\sqrt{3} + \sqrt{6}\alpha & 0 & 0 \\ 0 & 0 & 0 & 0 & 0 & 0 \\ 0 & 0 & 0 & 0 & 0 & 0 \end{bmatrix}, \quad (\text{D2})$$

$$S^z \simeq \frac{1}{6} \begin{bmatrix} 1 & 0 & -2\sqrt{2} + 2\alpha & 0 & 0 & 0 \\ -1 & 0 & 0 & -2\sqrt{2} + 2\alpha & 0 & 0 \\ 0 & -1 + \sqrt{2}\alpha & 0 & 0 & 0 & 0 \\ 0 & 0 & 1 - \sqrt{2}\alpha & 0 & 0 & 0 \\ 0 & 0 & 0 & 3 - 3\sqrt{2}\alpha & 0 & 0 \\ 0 & 0 & 0 & 0 & -3 + 3\sqrt{2}\alpha & 0 \end{bmatrix}. \quad (\text{D3})$$

Here, we have not shown the left bottom part of the matrices since they are all Hermitian matrices. For the t_{2g} spin operators \mathbf{S}_{ρ} 's,

$$S_{xy}^x \simeq \frac{1}{6} \begin{bmatrix} 0 & 1 & 0 & -\sqrt{2} + \alpha & 0 & 0 \\ 0 & \sqrt{2} - \alpha & 0 & 0 & 0 & 0 \\ 0 & 0 & -2 + 2\sqrt{2}\alpha & 0 & 0 & 0 \\ 0 & 0 & 0 & 0 & 0 & 0 \\ 0 & 0 & 0 & 0 & 0 & 0 \\ 0 & 0 & 0 & 0 & 0 & 0 \end{bmatrix}, \quad (\text{D4})$$

$$S_{xy}^y \simeq \frac{i}{6} \begin{bmatrix} 0 & 1 & 0 & -\sqrt{2} + \alpha & 0 & 0 \\ 0 & -\sqrt{2} + \alpha & 0 & 0 & 0 & 0 \\ 0 & 0 & -2 + 2\sqrt{2}\alpha & 0 & 0 & 0 \\ 0 & 0 & 0 & 0 & 0 & 0 \\ 0 & 0 & 0 & 0 & 0 & 0 \\ 0 & 0 & 0 & 0 & 0 & 0 \end{bmatrix}, \quad (\text{D5})$$

$$S_{zx}^y \simeq \frac{i}{6} \begin{bmatrix} 0 & -1 & 0 & \frac{-1}{\sqrt{2}} + \frac{\alpha}{2} & 0 & \frac{\sqrt{3}}{\sqrt{2}} - \frac{\sqrt{3}\alpha}{2} \\ 0 & \frac{-1}{\sqrt{2}} + \frac{\alpha}{2} & 0 & 0 & -\frac{\sqrt{3}}{\sqrt{2}} + \frac{\sqrt{3}\alpha}{2} & 0 \\ 0 & 0 & \frac{1}{2} - \frac{\alpha}{\sqrt{2}} & 0 & 0 & \frac{-\sqrt{3}}{2} + \frac{\sqrt{3}\alpha}{\sqrt{2}} \\ 0 & 0 & 0 & \frac{-\sqrt{3}}{2} + \frac{\sqrt{3}\alpha}{\sqrt{2}} & 0 & 0 \\ 0 & 0 & 0 & 0 & \frac{-3}{2} + \frac{3\alpha}{\sqrt{2}} & 0 \\ 0 & 0 & 0 & 0 & 0 & 0 \end{bmatrix}, \quad (\text{D11})$$

$$S_{xy}^z \simeq \frac{1}{6} \begin{bmatrix} -1 & 0 & -\sqrt{2} + \alpha & 0 & 0 & 0 \\ 1 & 0 & 0 & -\sqrt{2} + \alpha & 0 & 0 \\ -2 + 2\sqrt{2}\alpha & 0 & 0 & 0 & 0 & 0 \\ 2 - 2\sqrt{2}\alpha & 0 & 0 & 0 & 0 & 0 \\ 0 & 0 & 0 & 0 & 0 & 0 \\ 0 & 0 & 0 & 0 & 0 & 0 \end{bmatrix}, \quad (\text{D6})$$

$$S_{zx}^z \simeq \frac{1}{6} \begin{bmatrix} 1 & 0 & \frac{-1}{\sqrt{2}} + \frac{\alpha}{2} & 0 & -\frac{\sqrt{3}}{\sqrt{2}} + \frac{\sqrt{3}\alpha}{2} & 0 \\ -1 & 0 & \frac{-1}{\sqrt{2}} + \frac{\alpha}{2} & 0 & 0 & \frac{\sqrt{3}}{\sqrt{2}} - \frac{\sqrt{3}\alpha}{2} \\ \frac{1}{2} - \frac{\alpha}{\sqrt{2}} & 0 & 0 & \frac{\sqrt{3}}{2} - \frac{\sqrt{3}\alpha}{\sqrt{2}} & 0 & 0 \\ \frac{-1}{2} + \frac{\alpha}{\sqrt{2}} & 0 & 0 & 0 & \frac{\sqrt{3}}{2} - \frac{\sqrt{3}\alpha}{\sqrt{2}} & 0 \\ 0 & 0 & 0 & 0 & \frac{3}{2} - \frac{3\alpha}{\sqrt{2}} & 0 \\ 0 & 0 & 0 & 0 & 0 & \frac{-3}{2} + \frac{3\alpha}{\sqrt{2}} \end{bmatrix}. \quad (\text{D12})$$

$$S_{yz}^x \simeq \frac{1}{6} \begin{bmatrix} 0 & -1 & 0 & \frac{-1}{\sqrt{2}} + \frac{\alpha}{2} & 0 & \frac{-\sqrt{3}}{\sqrt{2}} + \frac{\sqrt{3}\alpha}{2} \\ 0 & \frac{1}{\sqrt{2}} - \frac{\alpha}{2} & 0 & 0 & \frac{-\sqrt{3}}{\sqrt{2}} + \frac{\sqrt{3}\alpha}{2} & 0 \\ 0 & 0 & \frac{1}{2} - \frac{\alpha}{\sqrt{2}} & 0 & 0 & \frac{\sqrt{3}}{2} - \frac{\sqrt{3}\alpha}{\sqrt{2}} \\ 0 & 0 & 0 & \frac{-\sqrt{3}}{2} + \frac{\sqrt{3}\alpha}{\sqrt{2}} & 0 & 0 \\ 0 & 0 & 0 & 0 & \frac{-3}{2} + \frac{3\alpha}{\sqrt{2}} & 0 \\ 0 & 0 & 0 & 0 & 0 & 0 \end{bmatrix}, \quad (\text{D7})$$

, Finally, we show the expression of the orbital angular momentum \mathbf{L} :

$$L_x \simeq \frac{1}{3} \begin{bmatrix} 0 & 2 & 0 & -\frac{1}{\sqrt{2}} + \frac{\alpha_L}{2} & 0 & -\frac{\sqrt{3}}{\sqrt{2}} + \frac{\sqrt{3}\alpha_L}{2} \\ 0 & \frac{1}{\sqrt{2}} - \frac{\alpha_L}{2} & 0 & 0 & -\frac{\sqrt{3}}{\sqrt{2}} + \frac{\sqrt{3}\alpha_L}{2} & 0 \\ 0 & 0 & 2 - \eta_L & 0 & 0 & -\sqrt{3} + \zeta_L \\ 0 & 0 & 0 & \sqrt{3} - \zeta_L & 0 & 0 \\ 0 & 0 & 0 & 0 & \sqrt{3} - \zeta_L & \kappa_L \\ 0 & 0 & 0 & 0 & 0 & 0 \end{bmatrix}, \quad (\text{D13})$$

$$S_{yz}^y \simeq \frac{i}{6} \begin{bmatrix} 0 & 1 & 0 & \frac{1}{\sqrt{2}} - \frac{\alpha}{2} & 0 & \frac{\sqrt{3}}{\sqrt{2}} - \frac{\sqrt{3}\alpha}{2} \\ 0 & \frac{1}{\sqrt{2}} - \frac{\alpha}{2} & 0 & 0 & -\frac{\sqrt{3}}{\sqrt{2}} + \frac{\sqrt{3}\alpha}{2} & 0 \\ 0 & 0 & \frac{-1}{2} + \frac{\alpha}{\sqrt{2}} & 0 & 0 & \frac{-\sqrt{3}}{2} + \frac{\sqrt{3}\alpha}{\sqrt{2}} \\ 0 & 0 & 0 & \frac{-\sqrt{3}}{2} + \frac{\sqrt{3}\alpha}{\sqrt{2}} & 0 & 0 \\ 0 & 0 & 0 & 0 & \frac{3}{2} - \frac{3\alpha}{\sqrt{2}} & 0 \\ 0 & 0 & 0 & 0 & 0 & 0 \end{bmatrix}, \quad (\text{D8})$$

$$L_y \simeq \frac{i}{3} \begin{bmatrix} 0 & 2 & 0 & -\frac{1}{\sqrt{2}} + \frac{\alpha_L}{2} & 0 & \frac{\sqrt{3}}{\sqrt{2}} - \frac{\sqrt{3}\alpha_L}{2} \\ 0 & -\frac{1}{\sqrt{2}} + \frac{\alpha_L}{2} & 0 & 0 & -\frac{\sqrt{3}}{\sqrt{2}} + \frac{\sqrt{3}\alpha_L}{2} & 0 \\ 0 & 0 & 2 - \eta_L & 0 & 0 & \sqrt{3} - \zeta_L \\ 0 & 0 & 0 & \sqrt{3} - \zeta_L & 0 & 0 \\ 0 & 0 & 0 & 0 & \sqrt{3} - \zeta_L & \kappa_L \\ 0 & 0 & 0 & 0 & 0 & 0 \end{bmatrix}, \quad (\text{D14})$$

$$S_{yz}^z \simeq \frac{1}{6} \begin{bmatrix} 1 & 0 & \frac{-1}{\sqrt{2}} + \frac{\alpha}{2} & 0 & \frac{\sqrt{3}}{\sqrt{2}} - \frac{\sqrt{3}\alpha}{2} & 0 \\ -1 & 0 & \frac{-1}{\sqrt{2}} + \frac{\alpha}{2} & 0 & 0 & \frac{-\sqrt{3}}{\sqrt{2}} + \frac{\sqrt{3}\alpha}{2} \\ \frac{1}{2} - \frac{\alpha}{\sqrt{2}} & 0 & 0 & \frac{-\sqrt{3}}{2} + \frac{\sqrt{3}\alpha}{\sqrt{2}} & 0 & 0 \\ \frac{-1}{2} + \frac{\alpha}{\sqrt{2}} & 0 & 0 & 0 & \frac{-\sqrt{3}}{2} + \frac{\sqrt{3}\alpha}{\sqrt{2}} & 0 \\ 0 & 0 & 0 & \frac{3}{2} - \frac{3\alpha}{\sqrt{2}} & 0 & 0 \\ 0 & 0 & 0 & 0 & \frac{-3}{2} + \frac{3\alpha}{\sqrt{2}} & 0 \end{bmatrix}, \quad (\text{D9})$$

$$L_z \simeq \frac{1}{3} \begin{bmatrix} 2 & 0 & -\sqrt{2} + \alpha_L & 0 & 0 & 0 \\ -2 & 0 & 0 & -\sqrt{2} + \alpha_L & 0 & 0 \\ 0 & 1 + \beta_L & 0 & 0 & 0 & 0 \\ 0 & 0 & -1 - \beta_L & 0 & 0 & 0 \\ 0 & 0 & 0 & -3 - \gamma_L & 0 & 0 \\ 0 & 0 & 0 & 0 & 3 + \gamma_L & 0 \end{bmatrix}, \quad (\text{D15})$$

$$S_{zx}^x \simeq \frac{1}{6} \begin{bmatrix} 0 & 1 & 0 & \frac{1}{\sqrt{2}} - \frac{\alpha}{2} & 0 & \frac{-\sqrt{3}}{\sqrt{2}} + \frac{\sqrt{3}\alpha}{2} \\ 0 & \frac{-1}{\sqrt{2}} + \frac{\alpha}{2} & 0 & 0 & \frac{-\sqrt{3}}{\sqrt{2}} + \frac{\sqrt{3}\alpha}{2} & 0 \\ 0 & 0 & -\frac{1}{2} + \frac{\alpha}{\sqrt{2}} & 0 & 0 & \frac{\sqrt{3}}{2} - \frac{\sqrt{3}\alpha}{\sqrt{2}} \\ 0 & 0 & 0 & \frac{-\sqrt{3}}{2} + \frac{\sqrt{3}\alpha}{\sqrt{2}} & 0 & 0 \\ 0 & 0 & 0 & 0 & \frac{3}{2} - \frac{3\alpha}{\sqrt{2}} & 0 \\ 0 & 0 & 0 & 0 & 0 & 0 \end{bmatrix}, \quad (\text{D10})$$

where $\kappa_L = \frac{9}{5}\varepsilon - \frac{9}{50}\varepsilon^2 + O(\varepsilon^3)$, $\eta_L = \frac{3}{5}\varepsilon + \frac{3}{50}\varepsilon^2 + O(\varepsilon^3)$, $\zeta_L = -\frac{3\sqrt{3}}{5}\varepsilon + \frac{3\sqrt{3}}{25}\varepsilon^2 + O(\varepsilon^3)$, and $\alpha_L = \frac{3\sqrt{2}}{5}\varepsilon - \frac{3}{50\sqrt{2}}\varepsilon^2 + O(\varepsilon^3)$, $\beta_L = \frac{12}{5}\varepsilon - \frac{3}{10}\varepsilon^2 - \frac{63}{250}\varepsilon^3 + O(\varepsilon^4)$, and $\gamma_L = -\frac{9}{50}\varepsilon^2 + O(\varepsilon^3)$.

-
- ¹ Y. Tokura and N. Nagaosa, *Science* **288**, 462 (2000).
- ² M. Fiebig, T. Lottermoser, D. Meier, and M. Trassin, *Nature Reviews Materials* **1**, 16046 (2016).
- ³ Y. Kuramoto, H. Kusunose, and A. Kiss, *J. Phys. Soc. Jpn.* **78**, 072001 (2009).
- ⁴ D. Pesin and L. Balents, *Nat. Phys.* **6**, 376 (2010).
- ⁵ G. Jackeli and G. Khaliullin, *Phys. Rev. Lett.* **102**, 017205 (2009).
- ⁶ J. Nasu, M. Udagawa, and Y. Motome, *Phys. Rev. Lett.* **113**, 197205 (2014).
- ⁷ P. Corboz, M. Lajkó, A. M. Läuchli, K. Penc, and F. Mila, *Phys. Rev. X* **2**, 041013 (2012).
- ⁸ K. Kitagawa, T. Takayama, Y. Matsumoto, A. Kato, R. Takano, Y. Kishimoto, S. Bette, R. Dinnebier, G. Jackeli, and H. Takagi, *Nature* **554**, 341 (2018).
- ⁹ T. Nomoto, K. Hattori, and H. Ikeda, *Phys. Rev. B* **94** (2016).
- ¹⁰ K. Hattori, T. Nomoto, T. Hotta, and H. Ikeda, *J. Phys. Soc. Jpn.* **86**, 113702 (2017).
- ¹¹ H. Watanabe, T. Shirakawa, and S. Yunoki, *Phys. Rev. Lett.* **110**, 027002 (2013).
- ¹² S. Vasala and M. Karppinen, *Prog. Solid State Chem.* **43**, 1 (2015).
- ¹³ J. Longo and R. Ward, *J. Am. Chem. Soc.* **83**, 2816 (1961).
- ¹⁴ C. R. Wiebe, J. E. Greedan, P. P. Kyriakou, G. M. Luke, J. S. Gardner, A. Fukaya, I. M. Gat-Malureanu, P. L. Russo, A. T. Savici, and Y. J. Uemura, *Phys. Rev. B* **68**, 134410 (2003).
- ¹⁵ A. W. Sleight, J. Longo, and R. Ward, *Inorganic Chemistry* **1**, 245 (1962), <https://doi.org/10.1021/ic50002a010>.
- ¹⁶ B. L. Chamberland and G. Lévassieur, *Mater. Res. Bull.* **14**, 401 (1979).
- ¹⁷ A. M. Abakumov, R. V. Shpanchenko, E. V. Antipov, O. I. Lebedev, and G. Van Tendeloo, *J. Solid State Chem.* **131**, 305 (1997).
- ¹⁸ C. R. Wiebe, J. E. Greedan, G. M. Luke, and J. S. Gardner, *Phys. Rev. B* **65** (2002).
- ¹⁹ K. G. Bramnik, H. Ehrenberg, J. K. Dehn, and H. Fuess, *Solid State Sci.* **5**, 235 (2003).
- ²⁰ K. Yamamura, M. Wakeshima, and Y. Hinatsu, *J. Solid State Chem.* **179**, 605 (2006).
- ²¹ C. A. Marjerrison, C. M. Thompson, G. Sala, D. D. Maharaj, E. Kermarrec, Y. Cai, A. M. Hallas, M. N. Wilson, T. J. S. Munsie, G. E. Granroth, R. Flacau, J. E. Greedan, B. D. Gaulin, and G. M. Luke, *Inorg. Chem.* **55**, 10701 (2016).
- ²² D. Hirai and Z. Hiroi, *J. Phys. Soc. Jpn.* **88**, 064712 (2019).
- ²³ H. Ishikawa, T. Takayama, R. K. Kremer, J. Nuss, R. Dinnebier, K. Kitagawa, K. Ishii, and H. Takagi, *Phys. Rev. B* **100**, 045142 (2019).
- ²⁴ A. Paramekanti, D. J. Singh, B. Yuan, D. Casa, A. Said, Y.-J. Kim, and A. D. Christianson, *Phys. Rev. B* **97**, 235119 (2018).
- ²⁵ J. H. Oh, J. H. Kim, J. H. Jeong, and S. H. Chang, *Curr. Appl. Phys.* **18**, 1225 (2018).
- ²⁶ A. Paramekanti, D. D. Maharaj, and B. D. Gaulin, *Phys. Rev. B* **101**, 054439 (2020).
- ²⁷ D. D. Maharaj, G. Sala, M. B. Stone, E. Kermarrec, C. Ritter, F. Fauth, C. A. Marjerrison, J. E. Greedan, A. Paramekanti, and B. D. Gaulin, *Phys. Rev. Lett.* **124**, 087206 (2020).
- ²⁸ K.-H. Ahn, K. Pajskr, K.-W. Lee, and J. Kuneš, *Phys. Rev. B* **95**, 064416 (2017).
- ²⁹ G. Chen, R. Pereira, and L. Balents, *Phys. Rev. B* **82**, 174440 (2010).
- ³⁰ L. Lu, M. Song, W. Liu, A. P. Reyes, P. Kuhns, H. O. Lee, I. R. Fisher, and V. F. Mitrović, *Nat. Commun.* **8**, 14407 (2017).
- ³¹ D. Hirai, H. Sagayama, S. Gao, H. Ohsumi, G. Chen, T.-h. Arima, and Z. Hiroi, *Phys. Rev. Research* **2**, 022063 (2020).
- ³² N. Iwahara and L. F. Chibotaru, *Phys. Rev. B* **107**, L220404 (2023).
- ³³ K. Hattori and H. Tsunetsugu, *J. Phys. Soc. Jpn.* **83**, 034709 (2014).
- ³⁴ K. Hattori and H. Tsunetsugu, *J. Phys. Soc. Jpn.* **85**, 094001 (2016).
- ³⁵ T. Ishitobi and K. Hattori, *Phys. Rev. B* **104**, L241110 (2021).
- ³⁶ H. Tsunetsugu, T. Ishitobi, and K. Hattori, *J. Phys. Soc. Jpn.* **90**, 043701 (2021).
- ³⁷ K. Hattori, T. Ishitobi, and H. Tsunetsugu, *Phys. Rev. B* **107**, 205126 (2023).
- ³⁸ T. Ishitobi and K. Hattori, *Phys. Rev. B* **107**, 104413 (2023).
- ³⁹ C. Svoboda, W. Zhang, M. Randeria, and N. Trivedi, *Phys. Rev. B* **104**, 024437 (2021).
- ⁴⁰ N. Iwahara, V. Vieru, and L. F. Chibotaru, *Phys. Rev. B* **98**, 075138 (2018).
- ⁴¹ X. Zhang, J. Zou, and G. Xu, (2023), [arXiv:2303.04010](https://arxiv.org/abs/2303.04010) [cond-mat.str-el].
- ⁴² Y. Shimizu, H. Takeda, M. Tanaka, M. Itoh, S. Niitaka, and H. Takagi, *Nat. Commun.* **3**, 981 (2012).